American Mineralogist, Volume 82, pages 888–899, 1997

Mobility of uranium during weathering

TAKASHI MURAKAMI,[1] TOSHIHIKO OHNUKI,[2] HIROSHI ISOBE,[2] AND TSUTOMU SATO[2]

[1]Mineralogical Institute, University of Tokyo, Bunkyo-ku, Tokyo 113, Japan
[2]Environmental Geochemistry Laboratory, Japanese Atomic Energy Research Institute, Tokai, Ibaraki 319-11, Japan

ABSTRACT

Mineralogical and geochemical mechanisms of U fixation under oxidizing conditions in the vicinity of the secondary U ore deposit at Koongarra, Australia, were examined using transmission and scanning electron microscopy and thermodynamic calculations. The formation of saléeite, $Mg(UO_2)_2(PO_4)_2 \cdot 10H_2O$, is the predominant mechanism for U fixation upstream from the deposit, where saléeite replaces sklodowskite and granular apatite. Within the deposit and further downstream, U is fixed in microcrystals (10–50 nm) of saléeite and (meta)torbernite scattered within veins of fine-grained (2–50 nm) Fe^{3+} minerals (primarily goethite and hematite). Thermodynamic calculations indicate the groundwater is undersaturated with respect to saléeite and metatorbernite and that these minerals should precipitate at higher U or P concentrations than observed. This suggests that the upstream saléeite precipitated at the reaction interfaces of dissolving sklodowskite and apatite under local saturation conditions. Observed textural relationships of saléeite and (meta)torbernite microcrystals with the Fe minerals, combined with thermodynamic calculations, suggest surface precipitation as the formation mechanism for saléeite and (meta)torbernite microcrystals within, and downstream from, the secondary ore deposit. Phosphorous released during the aging of ferrihydrite and U adsorbed onto Fe minerals are probably the sources of the major components of the microcrystals. Downstream, the microcrystals exist where groundwater U concentrations are as low as 10–30 μg/L. Once released from the ore deposit, U is fixed in uranyl phosphates even where measured groundwater is undersaturated with respect to uranyl phosphates. The surface precipitation is an important example of long-term post-adsorption U fixation in a natural system. The fully crystalline and radiation-damaged microstructures of saléeite indicate uranyl phosphates have formed continuously (or intermittently) for the last few million years.

INTRODUCTION

The two important oxidation states for U in natural waters are 4+ and 6+. The U^{4+} ion is essentially insoluble in mildly acidic to alkaline groundwaters, whereas U^{4+} solubility is commonly controlled by uraninite (see Table 1 for U mineral formulas and information) or cofinite. On the other hand, the U^{6+} ion is potentially much more mobile, due in part to the greater solubilities of most U^{4+} minerals (e.g., Osmond and Ivanovich 1992). Uranium dissolved in groundwater commonly forms complex ions, depending on geochemical conditions such as pH, Eh, and the presence of other dissolved ions (Langmuir 1978). The mobility of dissolved U in natural waters is affected by processes such as adsorption or desorption of U ions and precipitation or dissolution of U-bearing minerals. More complete information about the mechanisms of fixation and transport of U in groundwaters would enhance our understanding of the surficial U cycle (Gascoyne 1992).

Uranium sorption has been studied extensively, particularly U^{6+} sorption by Fe minerals at the Earth's surface (e.g., Tripathi 1983; Hsi and Langmuir 1985). Despite these studies, the chemical forms of U on solid substrates in natural systems are poorly understood, particularly at low U concentrations. Identifying the chemical forms of U is necessary for understanding the change in relationship between U and solid substrates after adsorption over a geologic time-scale, that is, long-term post-adsorption phenomena directly related to U mobility in natural systems. Waite et al. (1994) examined the chemical forms of U sorbed on ferrihydrite at pH 5 and 5.5 under atmospheric conditions using extended X-ray absorption fine structure (EXAFS) spectroscopy. They showed that mononuclear uranyl complexes on ferrihydrite surfaces share edges with Fe octahedra in ferrihydrite and no polynuclear uranyl complexes are evident as sorbed species, even at relatively high U concentration (approximately 20 mg/L). EXAFS studies of U^{6+} sorbed onto smectites led to different conclusions for local structures of UO_2^{2+} complexes, similar to those in solution (Dent et al. 1992) and distorted and distinct (Chisholm-Brause et al. 1994). In contrast, a laboratory experiment by Bruno et al. (1995) demonstrated schoepite can precipitate on the surfaces of Fe^{3+} oxyhydroxides following U sorption in 0.2–200 mg/L U solu-

0003–004X/97/0910–0888$05.00

TABLE 1. Selected U mineral species, formulas, and occurrences

Mineral species	Formula	Occurrence/age*
Autunite	$Ca(UO_2)_2(PO_4)_2 \cdot 10H_2O$	NF
Coffinite	$USiO_4 \cdot H_2O$	NF
Curite	$Pb_3U_8O_{27} \cdot 5H_2O$	UWZ/DW
Kasolite	$PbSiUO_6 \cdot 2H_2O$	UWZ/DW
Metaautunite	$Ca(UO_2)_2(PO_4)_2 \cdot 6H_2O$	NF
Metatorbernite	$Cu(UO_2)_2(PO_4)_2 \cdot 8H_2O$	WZ/DW
Renardite	$Pb(UO_2)_2(PO_4)_2(OH)_4 \cdot 7H_2O$	WZ/DW
Saléeite	$Mg(UO_2)_2(PO_4)_2 \cdot 10H_2O$	WZ/DW
Schoepite	$(UO_2)_8O_2(OH)_{12} \cdot 12H_2O$	NF
Sklodowskite	$(H_3O)_2Mg(UO_2)_2(PO_4)_2 \cdot 4H_2O$	UWZ†/DW
Torbernite	$Cu(UO_2)_2(PO_4)_2 \cdot 10H_2O$	WZ/DW
Uraninite	UO_{2+x}	UWZ/1.6 g.y.
Uranophane	$CaSi_2U_2O_{11} \cdot 6H_2O$	UWZ/DW

* NF = not found at Koongarra; UWZ = unweathered zone; DW = formed during weathering; WZ = weathered zone.
† Some sklodowskite is also found in the WZ.

tions. These studies addressed only short-term phenomena, and the long-term post-adsorption phenomena remain poorly understood in natural systems where U concentrations are commonly a few micrograms per liter.

Precipitation is another important mechanism by which U^{6+} is fixed in minerals. Uraninite, the most common primary mineral at U ore deposits, is not stable in waters under oxidizing conditions. Secondary U^{6+} minerals are frequently associated with U ore deposits (Rich et al. 1977) and have been observed at great distances from the primary source of U (Dall'aglio et al. 1974). Uraninite is altered not only to uranyl hydrates, but also to uranyl silicates, uranyl phosphates, or both, depending on water chemistries (e.g., Frondel 1958; Finch and Ewing 1992; Pearcy et al. 1995). Thus, U^{6+} can be fixed as U^{6+} minerals under certain conditions.

Vochten and his colleagues synthesized metatorbernite and metaautunite from concentrated U solutions and concluded that the formation of metatorbernite and metaautunite depends on the cations present in the solutions and on the physico-chemical conditions of U ore deposits (Vochten et al. 1979; Vochten and Deliens 1980). They demonstrated that this conclusion helps to explain the occurrence of torbernite, autunite, or both phases at oxidized U deposits such as Shinkolobwe (Zaire), Kobokobo (Zaire), and Margnac (France) (Vochten and Deliens 1980). On the other hand, inconsistent conclusions are drawn concerning the formation of kasolite at the Koongarra U ore deposit, Australia: Both direct precipitation from solution (Snelling 1980) and formation by replacement of sklodowskite (Isobe et al. 1992) have been proposed. Leo (1960) suggested that Ca and P from apatite are a source for autunite formation at Mt. Spokane, U.S.A; however, autunite is not observed at Koongarra, despite the presence of apatite. Instead saléeite is the common uranyl phosphate at Koongarra.

Recently, U transport in groundwaters has become of increasing concern for the long-term safety assessment of high-level nuclear-waste disposal sites (e.g., Airey and Ivanovich 1986). The long half-lives of the actinide elements present in nuclear waste necessitate that we understand the long-term migration behavior of these elements so that we may more accurately assess the long-term safety of a waste repository. Unfortunately, field observations and measurements of actinides, such as Pu, Np, and Am, are exceedingly difficult because of their low concentrations in natural groundwaters. Uranium migration away from a U ore deposit can provide deeper insight into actinide migration from a repository. Several U ore deposits, such as Cigar Lake, Canada (Philippe et al. 1993), Koongarra, Australia (Airey 1986), Peña-Blanca, Mexico (Pearcy et al. 1994), and Poços de Caldas, Brazil (Bruno et al. 1992), are sites of "natural analogue" studies where U transport has been examined in large-scale natural systems. Among these natural analogue sites, the Koongarra U ore deposit provides us with a large body of data on the geology, mineralogy, geochemistry, hydrogeology, and geomorphology collected by the International Alligator Rivers Analogue Project from 1987 to 1992 (e.g., Snelling 1992). These data provide a great opportunity to study U transport in nature.

This study focuses on the long-term post-adsorption phenomena and on the processes and mechanisms of U fixation. We report how U has been fixed in solid phases during the last million years under oxidizing conditions in the vicinity of the Koongarra U ore deposit, where the concentration of U in the groundwater is on the order of micrograms per liter. Adsorption and precipitation are included under the term fixation in the present study.

MINERALOGY, GEOCHEMISTRY, AND GEOLOGY AT KOONGARRA

The mineralogy, geochemistry, and geology at Koongarra have been investigated extensively (Snelling 1990; Edis et al. 1992; Murakami et al. 1992; Snelling 1992; Payne et al. 1992; Komninou and Sverjensky 1995a, 1995b; Koppi et al. 1996; Murakami et al. 1996). These studies are summarized briefly here.

Koongarra is located in a tropical monsoon climate. The host rock, a quartz-chlorite schist, and the primary U mineral, uraninite, currently at and near the surface have probably been subjected to weathering for more than one million years. (Airey et al. 1986). Quartz is resistant to weathering and persists even at the surface, whereas chlorite has been altered to vermiculite and kaolinite in the weathered zone (hereafter, referred to as WZ), which extends to about 25 m below the surface. Chlorite remains essentially unaltered in the unweathered zone (UWZ) below the WZ (Fig. 1). The conversion of chlorite with increased weathering is expressed: chlorite → vermiculite → kaolinite. The alteration of chlorite also produces Fe^{3+} minerals such as ferrihydrite, goethite, and hematite (Murakami et al. 1996); the conversion of chlorite occurs mainly in the transition zone (TZ) between the WZ and UWZ.

The Koongarra U ore deposit consists of primary and secondary ore deposits. The weathering that altered chlo-

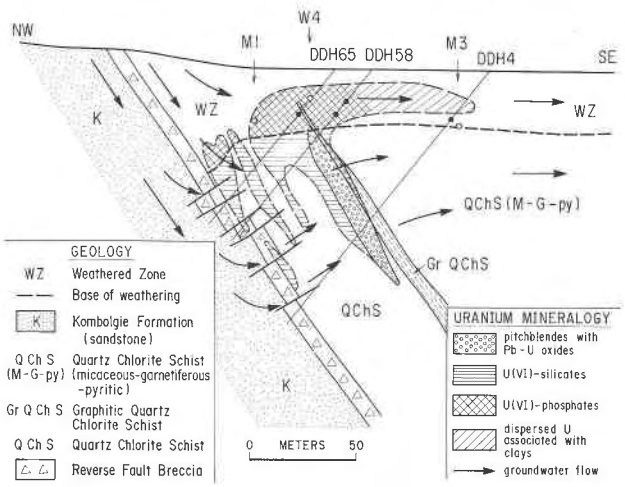

FIGURE 1. Schematic cross section to-scale of the Koongarra ore deposit (modified from Snelling 1980). The locations of the rock and water samples used for the present study are shown by solid and open circles, respectively. The core holes as well as the M1, W4, and M3 wells are in different cross sections but projected in this cross section where their locations are relatively arranged on the basis of the position of the graphitic quartz chlorite schist.

rite to the clay and Fe minerals simultaneously altered uraninite, which may still be occurring (Snelling 1992). In the primary ore deposit (30–100 m deep), uraninite has been partly altered to uranyl lead oxides such as curite and uranyl silicates, mainly sklodowskite (Snelling 1980; Isobe et al. 1992) (Fig. 1). The Koongarra reverse fault, formed at about 1600 m.y., has facilitated the alteration by providing a pathway of groundwater flow since the weathering started (Snelling 1992). In the secondary ore deposit (0–30 m deep), formed by weathering of the primary ore deposit, the uranyl oxides and silicates are further weathered, and U is found as uranyl phosphates, mostly saléeite (Snelling 1980; Isobe et al. 1994). However, the formation mechanism of saléeite is not well known. The redistribution of U downstream from the ore deposit is strongly affected by the weathering of chlorite: The weathered area has a higher concentration of U than does the unweathered area (Murakami et al. 1992). The U is most closely associated with secondary Fe minerals (Yanase et al. 1991). The same relationship between U concentration and Fe minerals was observed in the Ranger ore deposit, also located in the Alligator Rivers region (Lowson et al. 1986). However, the processes and mechanisms of U fixation into solid phases and the chemical forms of U-bearing materials have not been reported previously.

EXPERIMENTAL METHOD

The rock samples used in this study were collected from diamond-drill cores drilled upstream from, in the middle of, and downstream from the secondary ore deposit at Koongarra (Fig. 1). They are DDH65-92.5 (21.6 m depth from the surface); DDH65-95 (22.2 m) and DDH65-96 (22.4 m); DDH58-65 (15.2 m) and DDH58-91 (21.3 m); and DDH4-99 (23.1 m), respectively. The samples were collected in the TZ and WZ, and they mainly contain chlorite, quartz, and clay and Fe minerals. DDH65-92.5, DDH65-95, and DDH65-96 also contain U minerals. Concentrations in rocks are approximately 1000 mg/kg U upstream, 1000 mg/kg or more U in the middle, and 100–300 mg/kg U downstream (Edis et al. 1992). Concentrations in groundwaters are approximately 100, 100–400, and 10–30 μg/L U upstream, in the middle, and downstream, respectively (Payne et al. 1992).

Polished thin sections of the samples were examined by light microscopy, followed by scanning electron microscopy (SEM) with energy dispersive X-ray analysis (EDX) to identify the mineral species and to examine the textures of the samples. Because polished thin sections were used, backscattered-electron imaging (BEI) also was applied. A JEOL JSM-5400 and Hitachi S-4500 were used; both SEMs are equipped with EDX analyzers. The standard operating voltage was 15 kV, although 10 or 20 kV was also used when more detailed surface textures or higher-energy X-rays were needed, respectively.

To identify U-bearing phases within the Fe-mineral veins that are in contact with groundwater with low U concentration, sample DDH4-99 was examined further by high-resolution transmission electron microscopy (HRTEM) and analytical electron microscopy (AEM). After confirming the presence of U in the Fe-mineral veins of sample DDH4-99, a small piece of the Fe-mineral veins was removed from the thin section and subjected to ultramicrotomy after resin-impregnation, creating thin films less than 50 nm in thickness. The thin films were placed onto molybdenum or copper TEM grids. Saléeite crystals were extracted from samples DDH65-98.5 and DDH65-95 and examined by HRTEM and AEM. TEM samples for saléeite were prepared by grinding the saléeite crystals in ethanol and dispersing them onto holey carbon films attached to copper grids. A JEOL JEM 200CX, a JEOL JEM 2010, and a Hitachi HF 2000 were used for HRTEM and AEM examination.

We calculated the thermodynamic stabilities of saléeite, metatorbernite, and autunite in the current groundwater using the EQ3NR software package (Wolery 1992). Thermodynamic data were taken from Magalhaes et al. (1985) for saléeite ($\log K = -22.3$ at 25 °C) and metatorbernite ($\log K = -30.0$ at 25 °C), Read (1990) for autunite ($\log K = -19.43$ at 25 °C), Grenthe et al. (1992) for U^{6+} complexes in solution, and Wolery (1992) for the other dissolved and mineral species. The thermodynamic database for uranyl phosphate solids and soluble species may not be complete. For instance, we excluded data for $UO_2(HPO_4)_2^{2-}$ (in Langmuir 1978), which was critically discussed by Grenthe et al. (1992) and recommended by Bennett and Read (1992).

Groundwater compositions reported for wells M1, W4, and M3 by Payne (1992) were used for the thermodynamic calculations (Table 2). The locations of the M1,

Table 2. Water chemistries at Koongarra*

Location	M1	W4	M3	K. Cr.†
Depth (m)	24–26	13–15	26–28	—
pH	7.10	5.85	6.68	6.90
Eh (mV)	205	330	265	—
EC (μS/cm)	275	135	160	17
HCO_3^- (mg/L)	162	66	88	8
Cl^- (mg/L)	5.53	5.8	4.61	2.94
F^- (mg/L)	0.39	0.09	0.19	0.09
SO_4^{2-} (mg/L)	0.34	0.8	0.59	0.14
PO_4^{3-} (μg/L)	40	30	<5	25
Mg (mg/L)	21.9	12.3	13.2	0.46
Na (mg/L)	1.1	1.7	1.4	1.4
K (mg/L)	0.52	0.54	0.57	0.10
Ca (mg/L)	2.53	2.08	0.72	0.18
Si (mg/L)	4.3	9.8	11.5	3.9
Fe (μg/L)	7	17	16	133
Cu (μg/L)	—	0.62	—	—
Mn (μg/L)	120	421	104	7
U (μg/L)	128	414	28.8	0.21

* Data from Payne et al. (1992).
† K. Cr. = Koongarra Creek about 200 m from the ore deposit.

W4, and M3 wells (24–26, 13–15, and 26–28 m deep, respectively) are shown in Figure 1. The groundwater compositions for wells M1, W4, and M3 correspond to those upstream, in the middle, and downstream of the secondary ore deposit and thus relate to the water-rock interactions with DDH65-92.5, DDH65-95, and DDH65-96 upstream, DDH58-65 and DDH58-95 in the middle, and DDH4-99 downstream (Fig. 1). Well W4 has one of the highest U concentrations (414 μg/L) reported from Koongarra (Payne et al. 1992).

Activies of the solution species were calculated using the Davies equation. Calculated values of log (*Q/K*) for saléeite, metatorbernite, and autunite are given in Table 3 (*Q* is the activity product of species in a reaction).

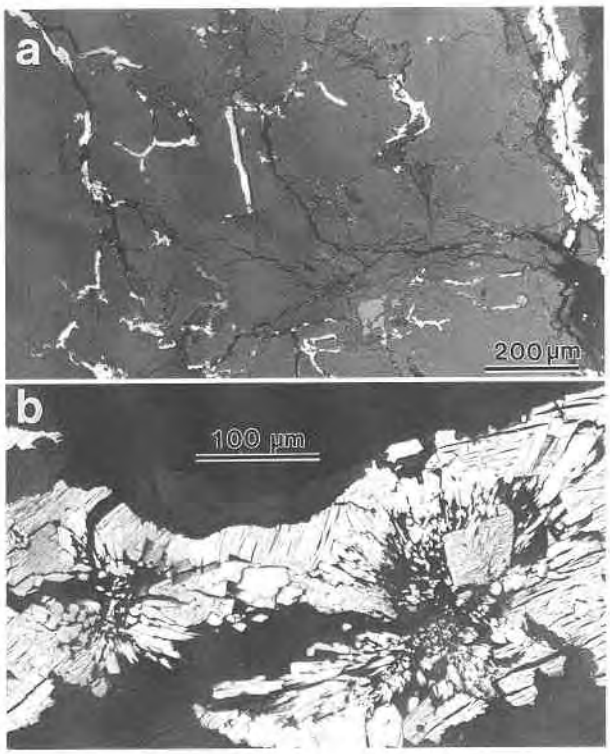

Figure 2. (**a**) Backscattered-electron image (BEI) of sklodowskite and saléeite in DDH65-92.5, occurring in microfissures and grain boundaries (brightest areas). The gray areas correspond to quartz, chlorite, and the weathered products. (**b**) BEI of saléeite in DDH65-95 growing in a sklodowskite vein. The difference in contrast between the two minerals is small but their textures are different; saléeite occupying most of the vein has fine cleavages and sklodowskite exhibits a radial texture.

Results

Uranium-bearing phases upstream of the secondary deposit

Sklodowskite is common in the primary ore deposit, and it also occurs, but rarely, upstream from the secondary ore deposit as veins within fissures and along grain boundaries (Fig. 2a). Examination of these "sklodowskite veins" indicates some of the sklodowskite is replaced by saléeite, where the remnant sklodowskite still retains its

Table 3. Values of log (*Q/K*) for saléeite, metatorbernite, and autunite at wells M1, W4, and M3

	Saléeite			Metatorbernite			Autunite
Condition	M1	W4	M3	M1*	W4	M3*	M1
As measured	−3.4	−0.58	−4.9	−7.8	−0.95	−7.8	−7.5
10 (P)†	−1.4	1.4	−2.9	−5.8	1.0	−6.0	−5.4
50 (P)	−0.019	2.8	−1.5	−4.4	2.4	−4.7	−4.0
100 (P)	0.58	3.4	−0.95	−3.8	3.0	−4.0	−3.4
10 (U)	−1.4	1.4	−2.9	−5.8	1.1	−6.0	−5.4
50 (U)	0.019	2.9	−1.5	−4.3	2.5	−4.6	−0.035
100 (U)	0.66	3.5	−0.92	−3.7	3.2	−4.0	0.61
100 (P) + 10 (U)	0.61	5.4	0.80	−1.8	5.1	−2.0	−1.4
10 (Cu)	NC	NC	NC	−6.8	0.041	−7.0	NC
50 (Cu)	NC	NC	NC	−6.1	0.74	−6.4	NC
100 (Cu)	NC	NC	NC	−5.8	1.0	−6.0	NC
100 (P) + 100 (Cu)	NC	NC	NC	−1.8	5.0	−2.0	NC
100 (P) + 100 (Ca)	NC	NC	NC	NC	NC	NC	−2.3

Note: NC means not calculated.
* Cu concentrations at wells M1 and M3 are not given in Payne et al. (1992). Therefore, the value in the M4 well was used in the calculations for all three wells.
† Concentration of the element in parentheses is ten times higher than the measured value; the following symbols should be read in a similar way.

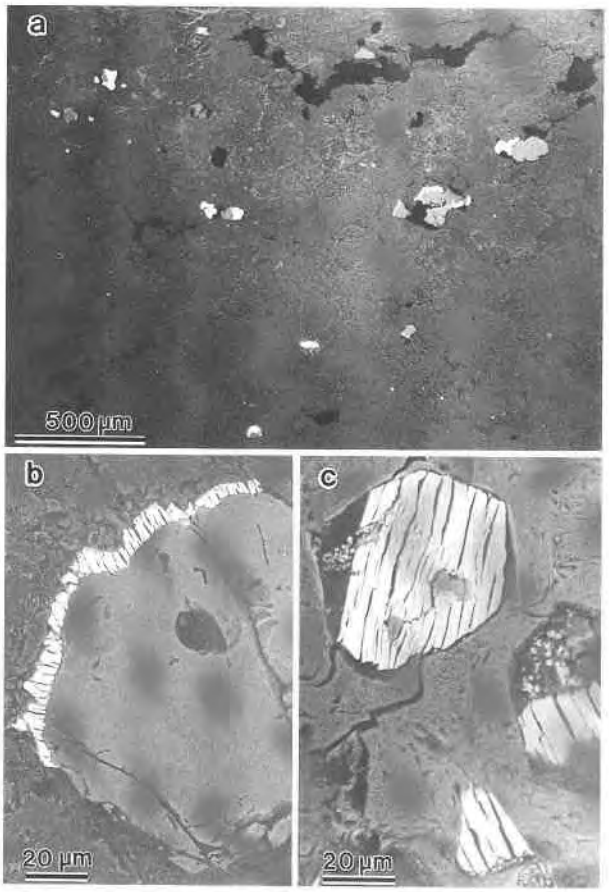

FIGURE 3. (**a**) BEI of saléeite (brightest areas) in DDH65-95 scattered among weathered quartz-chlorite schist. The gray areas accompanied by saléeite correspond to apatite. BEIs of saléeite (brightest area) in DDH65-95 (**b**) partly and (**c**) almost completely replacing apatite (gray, hexagonal shape).

original radial texture (Fig. 2b). Saléeite is also observed in veins without sklodowskite, which we interpret as being due to the complete replacement of sklodowskite by saléeite, with some sklodowskite constituents being dissolved in the groundwater. The presence of sklodowskite upstream from the secondary ore deposit suggests the original uraninite-bearing ore deposit existed at the level of the present WZ before the onset of weathering at Koongarra.

Saléeite is also found to be associated with apatite, an accessory mineral in the host rock (brightest areas in Fig. 3a). Closer examination reveals that apatite grains are partly or completely replaced by saléeite (Figs. 3b and 3c). The cavities in the apatite grains in Figure 3c indicate that some of apatite dissolved, and the dissolved constituents were transported downstream. The size of the saléeite aggregates is 20–100 μm. The replacement of apatite by autunite was not observed.

Figures 2b, 3b, and 3c reveal that saléeite crystals grew at the surface of sklodowskite or apatite at the expense of sklodowskite or apatite, respectively. The morphology

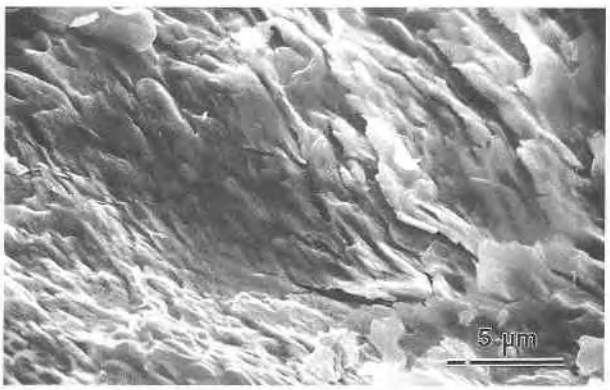

FIGURE 4. SEM image of the surface of saléeite (DDH65-95) upstream from the secondary ore deposit.

of the surface of the saléeite shows rounded cleavage surfaces (Fig. 4), suggesting the possibility of saléeite dissolution in some areas. No evidence for the formation of saléeite other than by the replacement of sklodowskite or apatite is observed upstream from the secondary ore deposit.

An unidentified uranyl vanadate with U:V= 1:1 containing Ti, K, and Ca, and another unidentified Ti-bearing phase with U:Ti = 2:1 containing V, K, and Ca were observed in the present study (sample DDH 65-92.5). They may be a mixture of a few phases. Uranium was also found in veins and along grain boundaries. These are associated with unidentified Pb-V, Fe, and Fe-Al phases with dimensions on the order of submicrometers to a few micrometers. We did not find additional uranyl phosphate such as metatorbernite or renardite as reported by Snelling (1980). Uranium-bearing phases other than saléeite are rare.

Two saléeite samples (DDH65-95 and DDH65-98.5) show distinct microstructures. The HRTEM image of saléeite in sample DDH65-95 shows no significant radiation damage and displays almost perfect two-dimensional lattice fringes in the $(0\bar{2}1)$ plane; there are no discontinuities apparent in the lattice fringes (Fig. 5a). Saléeite is monoclinic (a = 0.6951, b = 1.9947, c = 0.9896 nm, β = 135.17°); however, the Miller indices reported here refer to a pseudotetragonal unit cell ($a' \cong b' \cong$ 0.70 nm and $c' \cong$ 2.0 nm) (Miller and Taylor 1986). On the other hand, saléeite crystals in sample DDH65-98.5 show mainly intermediate metamict microstructures: Slightly to heavily distorted lattice fringes are observed with 1.0 and 0.35 nm spacings that correspond to (002) and (200), respectively (Fig. 5b). Lattice fringes with other crystallographic orientations in one crystal suggest that annealing of the radiation damage has occurred. The selected-area electron-diffraction (SAED) pattern shows faint diffraction spots and a diffuse diffraction halo (Fig. 5c), indicating the saléeite crystal in sample DDH65-98.5 contains both periodic and aperiodic domains. The microstructures and SAED pattern correspond to those observed in Stage II metamictization of zircon (Murakami et al. 1991). Some

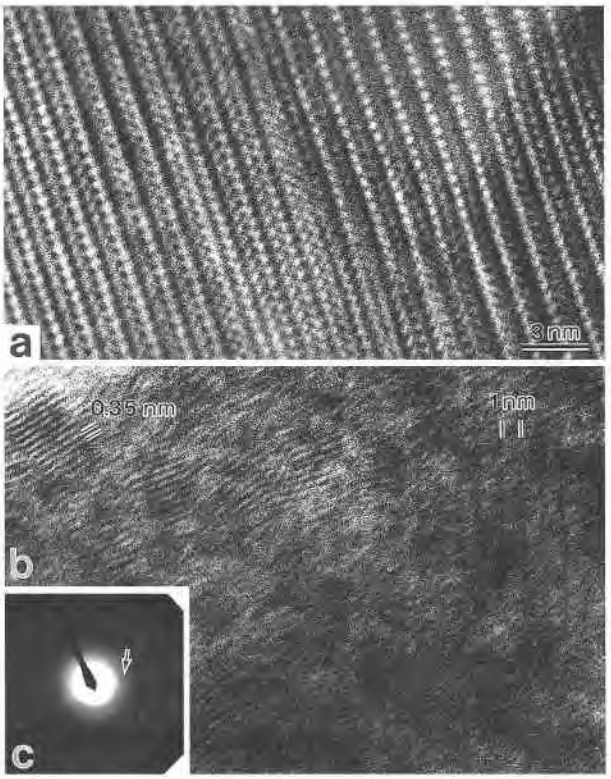

FIGURE 5. TEM images of saléeite; (**a**) ($0\bar{2}1$) plane showing a highly crystalline state, (**b**) lattice fringes of (002) and (200) (1.0 and 0.35 nm, respectively) indicating intermediate metamict microstructures, and (**c**) SAED pattern of the area including (**b**). The arrow indicates a 002 diffraction spot.

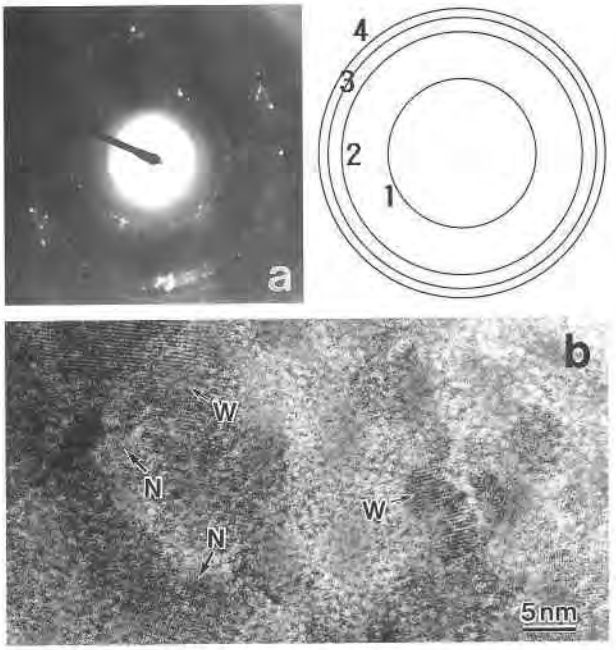

FIGURE 6. (**a**) SAED pattern of an Fe-mineral vein (left) and its schematic representation (right). The numbers are 1: d = 0.43 nm (110 of goethite); 2: d = 0.26 nm (130 of goethite and 104 of hematite); 3: d = 0.24 nm (111 of goethite and 110 of hematite); and 4: d = 0.22 nm (121 of goethite). (**b**) TEM image of a typical area of the Fe-mineral veins, showing that the area is mostly occupied by goethite and hematite. The wider lattice fringes of 0.43 nm correspond to (110) of goethite (e.g., smaller arrows labeled W), and the narrower lattice fringes of about 0.24 nm, correspond to (103), (111), or (121) of goethite, or (104) or (110) of hematite (e.g., larger arrows labled N).

grains of the saléeite in sample DDH65-98.5 show fully metamict microstructures, i.e., irregular contrast in the HRTEM images and a diffuse diffraction halo in the SAED pattern. The lattice fringes in Figure 5 demonstrate that saléeite retains its crystal structure under the high vacuum in the TEM.

Uranium-bearing phases downstream from the deposit

We identified U-bearing phases in the sample downstream from the deposit by HRTEM and AEM using the result of the reference saléeite. Therefore, we describe the downstream sample first, followed by those in the middle of the ore deposit. We use "(meta)torbernite" to denote metatorbernite or torbernite or a mixture, as torbernite could not be distinguished from metatorbernite by TEM in the present study.

Constituents of the Fe-mineral veins in sample DDH4-99, where we found U associated with P by SEM-EDX, were examined before identifying the U-bearing phases. One of the U-bearing areas was removed from the thin section and examined by TEM and AEM. The predominant crystalline phases in the Fe-mineral veins are goethite and hematite, since most of the diffraction spots and rings can be attributed to these two minerals (Fig. 6a), which agrees with the XRD result (Murakami et al. 1996). Ferrihydrite, which is difficult to identify using HRTEM or SAED, may coexist with goethite and hematite in this sample (Edis et al. 1992). An HRTEM micrograph indicates that the small domains of goethite and hematite (mostly in the range 2–50 nm) are randomly oriented (Fig. 6b). Those parts of the Fe-mineral domains lacking lattice fringes may correspond to amorphous material; however, some probably correspond to domains of goethite and hematite crystals that are not oriented with their primary zone axes parallel to the electron beam. Other domains with lattice fringes of 0.7 or 1.4 nm spacing, tentatively identified as chlorite, vermiculite, and kaolinite, are also found within the Fe-mineral veins, and their abundances are small. We did not find any direct association of U with chlorite, vermiculite, or kaolinite.

As with SEM and EDX examination, AEM indicates that U coexists with P, Mg, and Cu (Fig. 7a). Phosphorous, Mg, and Cu, are probably derived from dissolution of apatite, chlorite, and chalcopyrite of the host rock, respectively. Adjacent minerals, such as goethite and kaolinite, give rise to X-ray peaks for Al, Si, Fe, and Mg in the EDX spectrum (Fig. 7a). The U content of individual areas varies. Because saléeite and (meta)torbernite occur in the secondary ore deposit, the coexistence of U

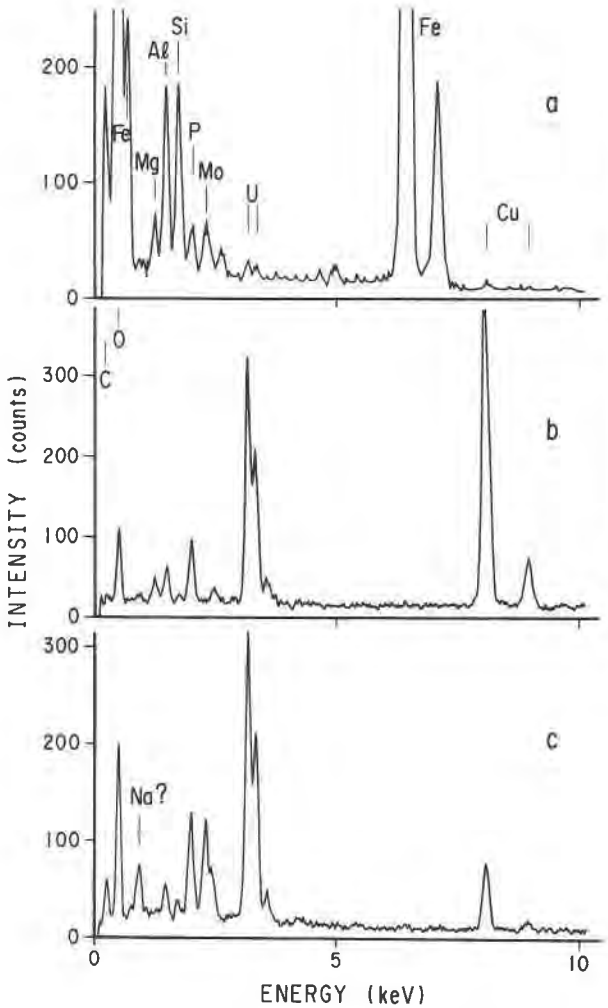

FIGURE 7. Spectra of (**a**) U-bearing area in an Fe-mineral vein in DDH4-99, (**b**) saléeite of DDH65-95, and (**c**) metatorbernite or torbernite from Bois Noirs, Massif Central, France. The C-coated samples were analyzed by AEM, on molybdenum TEM grids for (**a**) and (**c**) and on a copper TEM grid for (**b**).

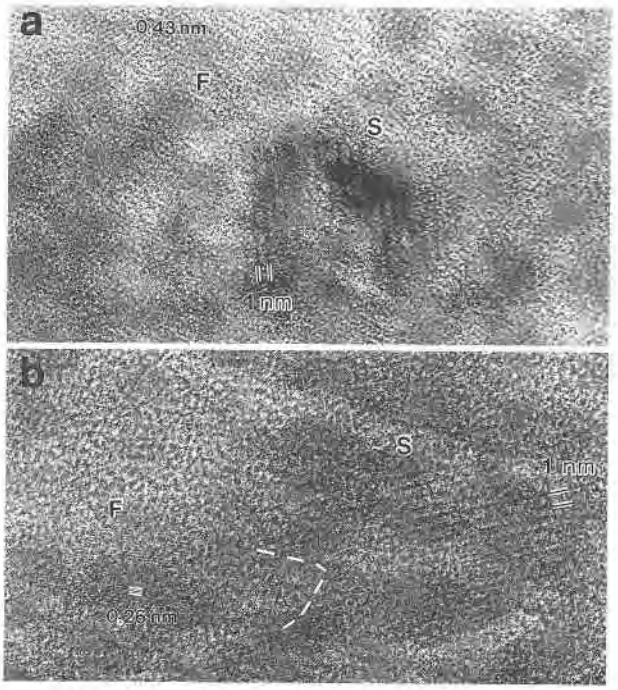

FIGURE 8. TEM images of (**a**) a saléeite domain (labeled S) among Fe minerals (e.g., labeled F, about 0.43 nm fringes), and (**b**) an anhedral saléeite domain (labeled S) coexisting with an Fe mineral (labeled F, about 0.26 nm fringes), shown with the interface between the two domains by a white, dashed line.

with P, Mg, and Cu suggests that saléeite and (meta)torbernite may occur as microcrystals. Figures 7b and 7c are EDX spectra for saléeite and (meta)torbernite, respectively, compared to the EDX spectrum from sample DDH4-99 (Fig. 7a). The X-ray peak ratios of P/U of the U-bearing areas (e.g., Fig. 7a) are usually larger than those of saléeite and (meta)torbernite (Figs. 7b and 7c), i.e., the Fe-mineral veins contain an additional amount of P compared to that needed for the probable formation of saléeite or (meta)torbernite. Indeed, P is detected among Fe minerals, even where U is absent.

The d_{002} value (1 nm) of saléeite is retained under high vacuum (Fig. 5); however, we did not have any metatorbernite or torbernite samples from Koongarra for comparison. Torbernite alters to metatorbernite at 75 °C by losing structurally bound H_2O (John 1984), but it is not known whether torbernite loses H_2O under high vacuum during TEM observation. We assume that the damaged microstructure of (meta)torbernite is similar to that of saléeite as in Figure 5b.

To confirm the presence of saléeite and (meta)torbernite among the Fe minerals, the U-bearing areas of the AEM samples were examined further by HRTEM. Domains of microcrystals (10–20 nm) are scattered between the Fe minerals. The microcrystals have lattice fringes of 1.0 nm ("S" in Fig. 8). These domains often show discontinuous, distorted lattice fringes, typical of radiation-damaged microstructures that are similar to those observed from saléeite in DDH65-98.5 (Fig. 5b). The domain labeled "S" at the center in Figure 8a displays two apparent sub-domains having the same crystallographic orientation, as indicated by the lattice fringes. The two sub-domains must have been continuous within a single microcrystal initially, being subsequently damaged by α-decay events. The *d* values and the radiation-damaged microstructures, along with the probable chemistry mentioned above, strongly indicate that the crystalline domains correspond to saléeite.

Although one domain of lattice fringes with spacing 0.85 nm, corresponding to (002) in metatorbernite (Stergiou et al. 1993), was observed, we could not identify metatorbernite with certainty, because of the small size of the microcrystal (4 nm). However, the possibility that (meta)torbernite is present cannot be excluded; both metatorbernite and torbernite are known to occur at Koon-

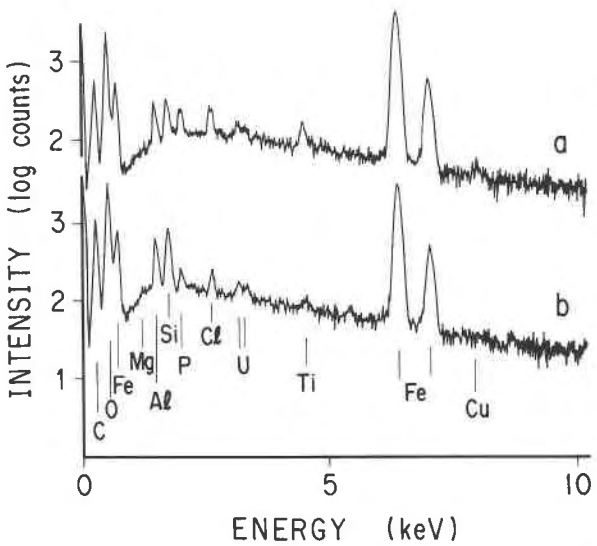

FIGURE 9. Spectra of Fe mineral veins of DDH58-65 (**a**) with low Mg, and (**b**) with low Cu. Both Mg and Cu are usually found with U in Fe mineral veins. The accelerating voltage was 20 kV.

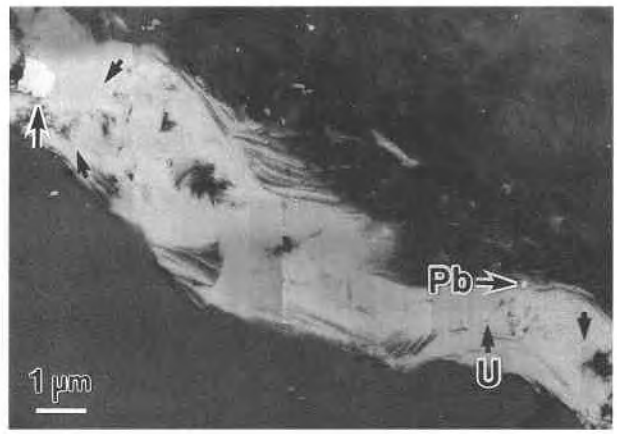

FIGURE 10. BEI of Fe mineral vein of DDH58-91. Bright areas in the Fe mineral vein are Pb-rich particles (larger arrows with white rims) and U-rich particles (smaller arrows without white rims). The size of the U-rich particles is consistent with those observed by HRTEM. The accelerating voltage was 10 kV. Arrows with U and Pb indicate analytical points by EDX, corresponding to Figures 11a and 11b, respectively.

garra (Snelling 1980), and U is almost always associated with Cu in these samples (Fig. 7a).

The textural relationship between saléeite and the Fe minerals is illustrated in Figure 8b. The saléeite domain of 20 nm ("S" in Fig. 8b) and the Fe mineral domain ("F" in Fig. 8b) are adjacent, and the interface between the two domains is clearly visible (the dashed white line in Fig. 8b). The saléeite domains are rounded ("S" in Figs. 8a and 8b). The probability that the neighboring saléeite and Fe mineral are both oriented with zone axes parallel to the incident electron beam (i.e., that the two minerals will display lattice fringes simultaneously) purely by chance is quite low; the saléeite domains themselves are rarely observed and are scattered among the Fe minerals. Thus the textural relationship between saléeite and the Fe mineral shown in Figure 8b provides information on the formation mechanism of saléeite and possibly (meta)torbernite downstream from the secondary ore deposit.

Uranium-bearing phases in the middle of the deposit

Iron-mineral veins fill fractures and microfissures in weathered quartz-chlorite schists and also occur within the gaps between the grain boundaries of quartz and chlorite. These Fe veins contain up to 2 wt% U according to SEM-EDX analyses. Because of the small sizes of the Fe-mineral veins (usually < 5 μm), SEM-EDX measurements are affected by neighboring minerals such as quartz and weathered chlorite (Fig. 9). In addition to U, the Fe-mineral veins contain P, Mg, and Cu. Uranium is always found with P and with either Cu or Mg (Figs. 9a and 9b, respectively), sometimes both. These qualitative analyses are consistent with the presence of saléeite and (meta)torbernite, as indicated by HRTEM and AEM examination of sample DDH4-99.

To verify whether saléeite and (meta)torbernite occur within the Fe-mineral veins, the SEM accelerating voltage was reduced to 10 kV. This reduces the region generating backscattered electrons and X-rays and reduces secondary fluorescence, thereby increasing resolution. Sklodowskite and saléeite show the higher contrast in BEI compared with the surrounding Fe minerals; this was confirmed in samples DDH65-92.5, DDH65-95, and DDH65-96.

Two types of bright areas of a typical Fe-mineral vein in Figure 10 display different compositions. One type of area is a few to several tens of nanometers in size and contains U (smaller arrows without white rims in Fig. 10 corresponding to the analysis in Fig. 11a). The second type contains approximately 0.1 and 1 μm regions that are rich in Pb (larger arrows with white rims in Fig. 10 corresponding to the analysis in Fig. 11b). The U-bearing particles contain Cu, Mg, and P in addition to U (Fig. 11a). Note that the EDX analyses (Figs. 11a and 11b) are affected by secondary fluorescence of surrounding materials. This combination of the BEI image and EDX analyses indicates nanometer-sized saléeite and (meta)torbernite microcrystals (approximately 20–50 nm) are present within Fe mineral veins in the middle of the secondary ore deposit.

DISCUSSION

Implication of microstructures for the age of saléeite formation

Damaged microstructures are caused by radiation doses accumulated by crystals that contain radioactive isotopes. An α-decay dose can be calculated as follows (Holland and Gottfried 1955):

$$D = 8N_1[\exp(\lambda_1 t) - 1] + 7N_2[\exp(\lambda_2 t) - 1] + 6N_3[\exp(\lambda_3 t) - 1],$$

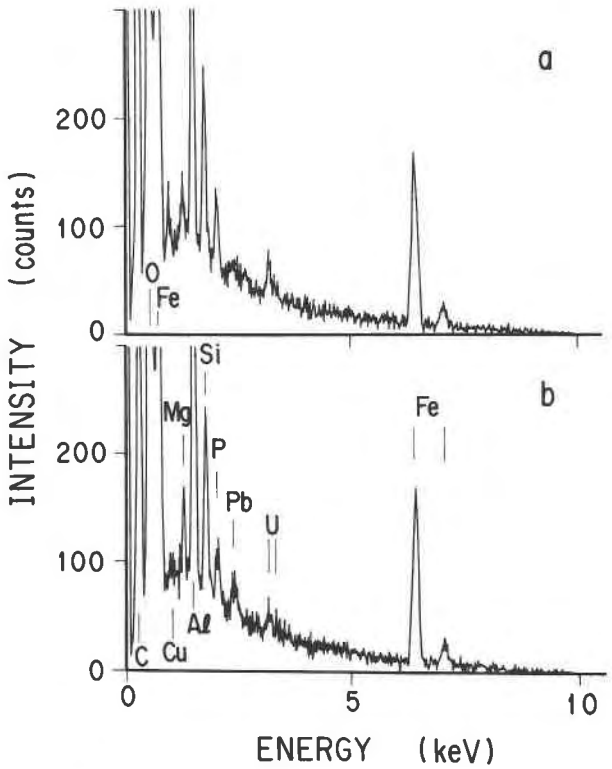

FIGURE 11. Spectra of Fe mineral vein of DDH58-91, from the areas of (**a**) the bright area indicated by an arrow with U in Figure 10, and (**b**) the bright area indicated by an arrow with Pb in Figure 10. Because the accelerating voltage was 10 kV, the relative intensities are changed; for instance, Cu$L\alpha$/Cu$K\alpha$ is about 100.

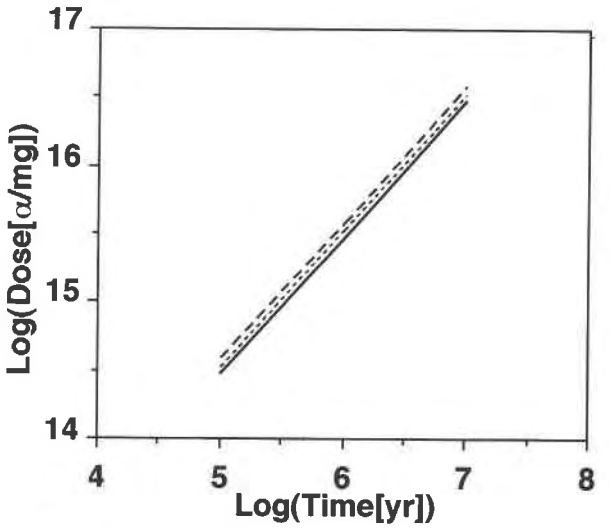

FIGURE 12. Calculated doses of saléeite with 60 wt% UO_3 (solid line), 65 wt% UO_3 (dotted line), and 70 wt% UO_3 (dashed line).

where D is the dose in α-decay events/mg; N_1, N_2, and N_3 are the present nuclide concentrations (atoms/mg), and λ_1, λ_2, and λ_3 are the decay constants (years^{-1}) for ^{238}U, ^{235}U, and ^{232}Th, respectively; t is the age of a sample in years. Dose increases with nuclide concentration and time. The second and third terms of the above equation contribute less than ~5% to the total calculated dose and can be neglected when estimating the radiation dose for saléeite since the time of its formation at Koongarra. The average Koongarra saléeite contains 64.8 wt% UO_3, with standard deviation of 1.2 wt% (Isobe et al. 1994). The radiation doses to Koongarra saléeites were calculated using UO_3 concentrations of 60, 65, and 70 wt% (Fig. 12). Figure 12 reveals that a wide range of doses in saléeite results from a range of formation ages and not from the U concentration variation.

The transition from the crystalline to the fully metamict state occurs within a narrow range of dose, 10^{15}–10^{16} α-decay events/mg (Ewing et al. 1987), and the intermediate metamict microstructures observed for the saléeites of samples DDH65-98.5 and DDH4-99 indicate that the saléeite samples upstream and downstream from the secondary ore deposit both have doses in this range. Doses of 10^{15}–10^{16} α-decay events/mg correspond to 5×10^5 to 4×10^6 years (Fig. 12) since the formation of saléeite. This is in good agreement with the age of the secondary mineralization estimated from radioactive decay-series disequilibria: $1–3 \times 10^6$ years (Airey et al. 1986). The effect of radiation-damage annealing in saléeite has been neglected, and the age calculated from the dose therefore represents a minimum age.

The presence of both fully crystalline and completely metamict saléeite indicates that saléeite in the secondary ore deposit began to form a few million years ago and has continued to form continuously or intermittently (Fig. 12). Radiation-damaged microstructures observed in saléeite downstream from the ore deposit suggest that the formation history and ages of saléeite downstream are similar to those of saléeite upstream.

Formation mechanism of saléeite upstream from the deposit

The calculated values of log (Q/K) of saléeite for all three well waters are less than 0, i.e., groundwater at Koongarra is currently undersaturated with respect to saléeite (Table 3). The calculations indicate that, even with the relatively high U concentration at the W4 well, saléeite will not precipitate. This result agrees with our observation that saléeite occurs only at particular sites, not along all water flow paths, such as fractures. It also agrees with our interpretation that saléeite is currently dissolving, as inferred from its morphology examined by SEM (Fig. 4).

However, the observation that, upstream from the secondary ore deposit, saléeite occurs only where sklodowskite and apatite have been replaced indicates that the local geochemical conditions in contact with sklodowskite and apatite crystals are sufficient to precipitate saléeite. We

estimated possible geochemical scenarios sufficient for the precipitation of saléeite, metatorbernite, and autunite.

Calculations were made based on the groundwater composition from the M1 well and changing pH from 5.85 to 7.3, an actual pH variation at Koongarra (Payne et al. 1992). The groundwater is still undersaturated with respect to saléeite in the above pH range. Thus, the presence of saléeite is not affected by the current pH variation, and therefore we exclude the pH variation from further discussion.

Calculations were then performed using the M1 water composition, but, for instance, with a U concentration ten times higher [10 (U) in Table 3]. Table 3 indicates that saléeite may be precipitated under conditions with higher U or P concentrations than those measured. Such conditions may be realized at the surfaces of sklodowskite and apatite, where U and P may be richer than in bulk groundwater because of the dissolution of the two minerals. The textural relationships between saléeite and sklodowskite and apatite (Figs. 2 and 3, respectively) and the thermodynamic calculations strongly suggest that saléeite is precipitated at the reaction interfaces of dissolving sklodowskite and apatite at the expense of U and P, respectively, by local saturation upstream of the secondary ore deposit.

Although uranophane, a Ca analogue of sklodowskite, is present in the primary ore deposit (Snelling 1980), autunite, the Ca analogue of saléeite, is absent in the secondary ore deposit. Table 3 shows that autunite is thermodynamically unstable in the groundwater at Koongarra, even if higher concentrations of U, P, or Ca were present, which is in contrast to the saléeite precipitation. This may explain why we observed saléeite instead of autunite replacing apatite. The U concentration in the Koongarra groundwater is not high enough for autunite to precipitate even at the surface of dissolving apatite.

Formation mechanism of U-bearing phases in the middle and downstream of the deposit

The apparent formation of U minerals in the middle or downstream of the secondary ore deposit could not be confirmed by naked eye or light microscopy from the present study. This is consistent with the undersaturation of the groundwaters at the W4 and M3 wells with respect to saléeite and metatorbernite (Table 3). Our thermodynamic calculations indicate that slightly higher concentrations of U, P, or Cu than that of the groundwater at the W4 well could facilitate saléeite or metatorbernite precipitation (Table 3), suggesting the possibility of local saturation (Snelling 1980). However, there are no such minerals as sklodowskite and apatite supplying sufficient ions for the formation of uranyl phosphates in the middle of the secondary ore deposit, resulting in little apparent uranyl phosphate formation by local saturation.

Despite the absence of uranyl phosphates visible to the naked eye, we showed evidence for microcrystals (10–50 nm) of saléeite and (meta)torbernite on Fe minerals in low-U concentration groundwater (as low as 10–30 μg/L). The uranyl phosphates were observed by HRTEM and high-resolution SEM although they were not evident using light microscopy or conventional SEM. The existence of saléeite and (meta)torbernite microcrystals among the Fe minerals (Figs. 8 and 10) is inconsistent with the local structures of UO_2^{2+} complexes sorbed to ferrihydrite (Waite et al. 1994) and smectite (Dent et al. 1992; Chisholm-Brause et al. 1994). Thus, adsorption alone cannot explain the formation. In addition the absence of sklodowskite and apatite in the middle and downstream of the secondary ore deposit and the thermodynamic calculations (Table 3) strongly suggest that simple solubility-controlled precipitation cannot explain the formation either.

Even if the bulk solution is undersaturated with respect to saléeite and (meta)torbernite, the TEM observations suggest that a high density of U, P, and Mg or Cu, enough to form saléeite and (meta)torbernite, must be attained at the surface of Fe mineral microcrystals. The Fe minerals are formed during chlorite weathering (Murakami et al. 1996), and ferrihydrite is the first to form among the Fe minerals. Phosphorous in groundwater is sorbed onto ferrihydrite by adsorption or coprecipitation. This is consistent with the fact that an additional amount of P compared to that needed for the formation of uranyl phosphates is contained in the Fe minerals (Fig. 7a). The P incorporated in ferrihydrite may be released during the aging of ferrihydrite to goethite and hematite in the same way that As^{5+} is released during the crystal growth of ferrihydrite (Fuller et al. 1993). Such P is probably the source of saléeite and (meta)torbernite rather than P in groundwater. Along with such P, adsorbed U onto Fe minerals could result in surface precipitation, a possible formation mechanism of saléeite and (meta)torbernite microcrystals at the surface of Fe minerals [for instance, see the saturation of saléeite with 100(P) and 10(U) at the M3 well in Table 3].

Thus, the formation occurs in a limited and particular area, i.e., at the surface of Fe mineral microcrystals. The U fixation mechanism is the same in the middle and downstream of the secondary ore deposit, i.e., the formation of uranyl phosphates. The formation mechanism proposed here may be slightly different from that reported by Bruno et al. (1995) who showed that surface precipitation of schoepite is possible on ferric oxyhydroxide following adsorption of U^{6+}. Our proposed mechanism requires that at least P must be derived from the Fe minerals.

Sato et al. (1997) recently found Fe nodules in the middle of the secondary ore deposit. They report that the Fe nodules contain up to 8% U, and a high correlation between U, P, and Cu implies the existence of (meta)torbernite microcrystals. The (meta)torbernite formation within Fe nodules is consistent with our results. Thus, the formation of microcrystals of saléeite and (meta)torbernite demonstrates that long-term post-adsorption phenomena actually occur in natural systems with

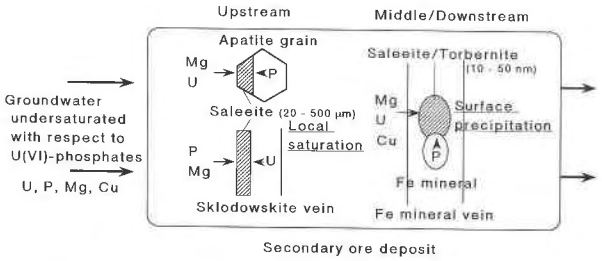

FIGURE 13. Schematic diagram summarizing U fixation mechanisms in the vicinity of the secondary ore deposit.

groundwater U concentrations on the order of micrograms per liter.

The fixation mechanism of U in the vicinity of the secondary ore deposit is by formation of the uranyl phosphates saléeite and (meta)torbernite. However, the formation mechanisms of the uranyl phosphates are quite different, depending on location with respect to the secondary ore deposit. Koongarra groundwater contains Mg, U, and P released from chlorite, U minerals, and apatite, respectively, and flows through the secondary ore deposit (Fig. 13). Saléeite replaces sklodowskite and apatite by local supersaturation upstream, and in the middle and downstream, microcrystals (1–50 nm) of saléeite and (meta)torbernite are formed at the surface of Fe minerals by surface precipitation even where groundwater U concentrations are low (approximately 30 μg/L). This process has occurred over the last few million years.

ACKNOWLEDGMENTS

The authors are indebted to P. Duerden and A.A. Snelling for the collection of the samples, and to H. Momoi, H. Asada, and T. Minakawa at Ehime University for discussions. One of the authors (T.M.) thanks K. Tsuzuki and J. Kiyoshige for their patient TEM and SEM work when they were students of T.M. R.J. Finch is gratefully acknowledged for his comments on an earlier version of the manuscript. The authors thank the reviewers J. Bruno, M.C. Duff, and K.L. Nagy for their helpful comments. Part of the electron microprobe analysis and electron microscopy was performed in the Electron Microbeam Analysis Facility of the Mineralogical Institute, University of Tokyo. Part of the present study was supported by a Scientific Grant of the Ministry of Education, Science and Culture (No. 6640620).

REFERENCES CITED

Airey, P.L. (1986) Radionuclide migration around uranium ore bodies in the Alligator Rivers Region of the Northern Territory of Australia—Analogue of radioactive waste repositories—A review. Chemical Geology, 55, 255–268.

Airey, P.L. and Ivanovich, M. (1986) Geochemical analogues of high-level radioactive waste repositories. Chemical Geology, 55, 203–213.

Airey, P.L., Golian, C., and Lever, D.A. (1986) An approach to the mathematical modelling of the uranium series redistribution within ore bodies: Topical Report AAEC/C49, 106 p. Australian Nuclear Science and Technology Organisation, Sydney.

Bennet, D.G. and Read, D. (1992) Geochemical data bases, Alligator Rivers Analogue Project Final Report 10, DOE/HMIP/RR/92/080, 56 p. Australian Nuclear Science and Technology Organisation, Sydney.

Bruno, J., Cross, J.E., Eikenberg, J., McKinley, I., Read, D., Sandino, A., and Selllin, P.J. (1992) Testing models of trace element geochemistry at Poços de Caldas. Journal of Geochemical Exploration, 45, 451–470.

Bruno, J., De Pablo, J., Duro, L., and Figuerola, E. (1995) Experimental study and modeling of the U(VI)-Fe(OH)$_3$ surface precipitation/coprecipitation equilibria. Geochimica et Cosmochimica Acta, 59, 4113–4123.

Chisholm-Brause, C., Conradson, S.D., Buscher, C.T., Eller, P.G., and Morris, D.E. (1994) Speciation of uranyl sorbed at multiple binding sites on montmorillonite. Geochimica et Cosmochimica Acta, 58, 3625–3631.

Dall'aglio, M., Gragnani, N., and Locardi, E. (1974) Geochemical factors controlling the formation of the secondary minerals of uranium. In Formation of Uranium Ore Deposits, p. 33–48. International Atomic Energy Agency, Vienna.

Dent, A.J., Ramsay, J.D.F., and Swanton, S.W. (1992) An EXAFS study of uranyl ion in solution and sorbed onto silica and montmorillonite clay colloids. Journal of Colloid and Interface Science, 150, 45–60.

Edis, R., Cao, L., Cashion, J., Klessa, D., Koppi, A.J., Murakami, T., Nightingale, T., Payne, T., Snelling, A., and Yanase, N. (1992) Chemistry and mineralogy of rocks and soils, Alligator Rivers Analogue Project Final Report 8, ISBN 0-642-59934-3, 255 p. Australian Nuclear Science and Technology Organisation, Sydney.

Ewing, R.C., Chakoumakos, B.C., Lumpkin, G.R., and Murakami, T. (1987) The metamict state. MRS Bulletin, 12, 58–66.

Finch, R.J. and Ewing, R.C. (1992) The corrosion of uraninite under oxidizing conditions. Journal of Nuclear Materials 190, 133–156.

Frondel, C. (1958) Systematic Mineralogy of Uranium and Thorium. U.S. Geological Survey Bulletin 1064, 400 p.

Fuller, C.C., Davis, J.A., and Waychunas, G.A. (1993) Surface chemistry of ferrihydrite: Part 2. Kinetics of arsenate adsorption and coprecipitation. Geochimica et Cosmochimica Acta, 57, 2271–2282.

Gascoyne, M. (1992) Geochemistry of the actinides and their daughters. In M. Ivanovich and R.S. Harmon, Eds., Uranium-series disequilibrium: Applications to earth, marine, and environmental sciences (2nd Ed.), p. 34–61. Oxford University Press, Oxford.

Grenthe, I., Fuger, J., Konings, R.J.M., Lemire, R.J., Muler, A.B., Nguyen-Trung, C., and Wanner, H. (1992) In H. Wanner and I. Forest, Eds., Chemical Thermodynamics of Uranium, 715 p. Elsevier, Amsterdam.

Holland, H.D. and Gottfried, D. (1955) The effect of nuclear radiation on the structure of zircon. Acta Crystallographica, 8, 291–300.

Hsi, C-K.D. and Langmuir, D. (1985) Adsorption of uranyl onto ferric oxyhydroxides: Application of the surface complexation site-binding model. Geochimica et Cosmochimica Acta, 49, 1931–1941.

Isobe, H., Murakami, T., and Ewing, R.C. (1992) Alteration of uranium minerals in the Koongarra deposit, Australia: Unweathered zone. Journal of Nuclear Materials 190, 174–187.

Isobe, H., Ewing, R.C., and Murakami, T. (1994) Formation of secondary uranium minerals in the Koongarra deposit, Australia. Materials Research Society Symposium Proceedings, 333, 653–660.

John, D. (1984) Phase relations and crystal chemistry of secondary uranium minerals of the torbernite group. 203 p. Ph.D. thesis, Victoria University of Manchester.

Komninou, A. and Sverjensky, D.A. (1995a) Pre-ore hydrothermal alteration in an unconformity-type uranium deposit. Contribution to Mineralogy and Petrology, 121, 99–114.

——— (1995b) Hydrothermal alteration and the chemistry of ore-forming fluids in an unconformity-type uranium deposit. Geochimica et Cosmochimica Acta, 59, 2709–2723.

Koppi, A. J., Edis, R., Field, D.J., Geering, H.R., Klessa, D.A., and Cockayne, D.J.H. (1996) Rare earth element trend and cerium-uranium-manganese associations in weathered rock from Koongarra, Northern Territory, Australia. Geochimica et Cosmochimica Acta, 60, 1695–1707.

Langmuir, D. (1978) Uranium solution-mineral equilibria at low temperatures with applications to sedimentary ore deposits. Geochimica et Cosmochimica Acta, 42, 547–569.

Leo, G.W. (1960) Autunite from Mt. Spokane. American Mineralogist, 45, 99–128.

Lowson, R.T., Short, S.A., Davey, B.G., and Gray, D.J. (1986) $^{234}U/^{238}U$ and $^{230}Th/^{234}U$ activity ratios in mineral phases of a lateritic weathered zone. Geochimica et Cosmochimica Acta, 50, 1697–1702.

Magalhaes, M.C.F., Pedrosa de Jesus, J.D., and Williams, P.A. (1985) The chemistry of uranium dispersion in groundwaters at the Pinhal do Souto mine, Portugal. Inorganica Chimica Acta 109, 71–78.

Miller, S.A. and Taylor, J.C. (1986) The crystal structure of saléeite, $Mg[UO_2PO_4]_2 \cdot 10H_2O$. Zeitschrift für Kristallographie, 177, 247–253.

Murakami, T., Chakoumakos, B.C., Ewing, R.C., Lumpkin, G.R., and Weber, W.J. (1991) Alpha-decay event damage in zircon. American Mineralogist, 76, 1510–1532.

Murakami, T., Isobe, H., Ohnuki, T., Yanase, N., Sato, T., Kimura, H., Sekine, K., Edis, R., Koppi, A.J., Klessa, D.A., Conoley, C., Nagano, T., Nakashima, S., and Ewing, R.C. (1992) Weathering and its effects on uranium redistribution, Alligator Rivers Analogue Project Final Report 9, ISBN 0-642-59935-1, 138 p. Australian Nuclear Science and Technology Organisation, Sydney.

Murakami, T., Isobe, H., Sato, T., and Ohnuki, T. (1996) Weathering of chlorite in a quartz-chlorite schist: I. Mineralogical and chemical changes. Clays and Clay Minerals, 44, 244–256.

Osmond, J.K. and Ivanovich, M. (1992) Uranium-series mobilization and surface hydrology. In M. Ivanovich and R.S. Harmon, Eds., Uranium-series disequilibrium: Applications to earth, marine, and environmental sciences (2nd Ed.), p. 259–289. Oxford University Press, Oxford.

Payne, T.E., Edis, R., Herczeg, A.L., Sekine, K., Seo, Y., Waite, T.D., and Yanase, N. (1992) Groundwater chemistry, Alligator Rivers Analogue Project Final Report, 7, ISBN 0-642-59933-5, 185 p. Australian Nuclear Science and Technology Organisation, Sydney.

Pearcy, E.C., Prikryl, J.D., Murphy, W.M., and Leslie, B.W. (1994) Alteration of uraninite from the Nopal-I deposit, Peña-Blanca District, Chihuahua, Mexico, compared to degradation of spent nuclear fuel in the proposed United-States high-level nuclear waste repository at Yucca Mountain, Nevada. Applied Geochemistry, 9, 713–732.

Pearcy, E.C., Prikryl, J.D., and Leslie, B.W. (1995) Uranium transport through fractured silicic tuff and relative retention in areas with distinct fracture characteristics. Applied Geochemistry, 10, 685–704.

Philippe, S., Lancelot, J.R., Clauer, N., and Pacquet, A. (1993) Formation and evolution of the Cigar Lake uranium deposit based on U-Pb and K-Ar isotope systematics. Canadian Journal of Earth Sciences 30, 720–730.

Read, D. (1990) Chemical project report on stage 2: Application of speciation models to laboratory and field data sets, EUR-13124, 231 p. Commission of the European Communities.

Rich, R.A., Holland, H.D., and Peterson, U. (1977) Hydrothermal Uranium deposits, Developments in economic geology, 6, 264 p. Elsevier, Amsterdam.

Sato, T., Murakami, T., Yanase, N., Isobe, H., Payne, T.E., and Airey, P.L. (1997) Iron nodules scavenging uranium from groundwater. Environmental Science and Technology, in press.

Snelling, A A. (1980) Uraninite and its alteration products, Koongarra uranium deposit. In J. Ferguson and A.B. Goleby, Eds., Uranium in the Pine Creek Geosyncline, p. 487–498. International Atomic Energy Agency, Vienna.

———(1990) Koongarra uranium deposits. In F.E. Hughes, Ed., The geology of the mineral deposits of Australia and Papua New Guinea, p. 807–812. The Australian Institute of Mining and Metallurgy, Melbourne.

———(1992) Geologic setting, Alligator Rivers Analogue Project Final Report 2, ISBN 0-642-59928-9, 118 p. Australian Nuclear Science and Technology Organisation, Sydney.

Stergiou, A.C., Rentzeperis, P.J., and Sklavounos, S. (1993) Refinement of the crystal structure of metatorbernite. Zeitschrift für Kristallographie, 205, 1–7.

Tripathi, V.S. (1983) Uranium(VI) transport modelling: Geochemical data and submodels. 297 p. Ph.D. dissertation, Stanford University, Palo Alto, California.

Vochten, R. and Deliens, M. (1980) Transformation of curite into metaautunite paragenesis and electrokinetic properties. Physics and Chemistry of Minerals, 6, 129–143.

Vochten, R., Huybrechts, W., Remaut, G., and Deliens, M. (1979) Formation of meta-torbernite starting from curite: Crystallographic data and electrokinetic properties. Physics and Chemistry of Minerals, 4, 281–290.

Waite, T.D., Davis, J.A., Payne, T.E., Waychunas, G.A., and Xu, N. (1994) Uranium(VI) adsorption to ferrihydrite: Application of a surface complexation model. Geochimica et Cosmochimica Acta, 58, 5465–5478.

Wolery, T.J. (1992) EQ3NR, A computer program for geochemical aqueous speciation-solubility calculations: Theoretical manual, user's guide, and related documentation (version 7.0), UCRL-MA-110662 PT III, 246 p. Lawrence Livermore Laboratory, University of California.

Yanase, N., Nightingale, T., Payne, T., and Duerden, P. (1991) Uranium distribution in mineral phases of rock by sequential extraction procedure. Radiochimica Acta, 52/53, 387–393.

Manuscript received October 21, 1996
Manuscript accepted May 1, 1997